

# Granular Graphene: direct observation of zigzag and armchair edge waves

Li-Yang Zheng,\* Florian Allein, Vincent Tournat, Vitalyi Gusev, and Georgios Theocharis†  
LAUM, UMR-CNRS 6613, Le Mans Université, Av. O. Messiaen, 72085 Le Mans, France

(Dated: December 15, 2024)

We propose a mechanical granular graphene obtained by replacing the carbon atoms with macroscopic spherical stainless steel beads in contact. The experimentally measured dispersion relation is presented, in conjunction with evidence of the Dirac points. In addition, wave propagation along the zigzag and a robust turning effect of edge waves from the zigzag to the armchair boundary is experimentally revealed, even in the absence of a full band gap for bulk modes. Our work shows that mechanical granular graphene can serve as an excellent experimental platform to study novel Dirac, topological and nonlinear wave phenomena.

Graphene [1–3] has recently emerged as an appealing system for conducting fundamental studies in condensed matter physics and Dirac physics phenomena. Genuine graphene supports electronic edge states, which play an important role in showcasing the fascinating transport properties of graphene nanoribbons [4]. The existence of electronic states localized at its zigzag boundary has been confirmed by scanning-tunneling microscopy. The armchair boundaries do not support electronic edge states unless defects appear on the edge [5]. Regarding phonon edge states, theoretical studies on genuine graphene [6] have shown that phonon zigzag and armchair edge states are possible, but no experimental evidence has been produced so far.

Due to the difficulty in modifying graphene at will at the nanoscale, researchers have proposed other artificial microscopic and macroscopic honeycomb structures to study further Dirac physics phenomena. These settings include the use of molecules [7], ultracold atoms [8], photons [9–13] or phonons [14, 15]. An extensive body of works has been published over the last few years, studying the edge states in different artificial graphene structures [16–22]. Experimentally, the only report on armchair edge waves is in a photonic graphene-like structure of coupled micropillars [23], where the existence of edge wave is due to the couplings of  $p_{x,y}$  photonic orbitals based on the tight-binding model [17].

In this work, we propose another type of artificial graphene, namely granular graphene, which can be thought of as a mechanical graphene whose carbon atoms have been replaced by macroscopic elastic beads and chemical bonds replaced by contact interactions via various stiffnesses. Similar to genuine graphene or other mechanical graphene structures [24], the granular graphene also exhibits Dirac cones [25, 26], and other interesting Dirac physics phenomena, such as an analogue of the quantum spin Hall effect [27]. However, the granular graphene possesses extra physical features that make it very appealing. These features include: (i) the existence of multiple degrees of freedom (translations and rotations) [28–31] which enrich its dispersion relation; and (ii) access to nonlinear dynamics leading to the nonlinear phenomena like solitons [32, 33], nonlinear waves [34–

38] and breathers [39, 40]. In addition, it has been shown that various kinds of edge states [41] are supported. Thus far however, no direct observation has been made of Dirac cones or edge wave propagation on granular graphene. The challenges lie in constructing a stable and reliable two-dimensional (2D) granular crystal that behaves like the free-standing one. Previous reports from 2D granular crystal studies have focused on closely-packed hexagonal or square lattices with mechanical constraints located on the borders [42–44].

This article presents how such structural difficulties have been overcome using periodic external magnetic fields. The proposed magneto-granular graphene (MGG) is structurally stable and acts as a nearly free-standing granular structure. We experimentally show the dispersion curves, evidence of the Dirac point, and direct observations of the edge wave propagation in the MGG. More importantly, a turning effect of edge waves from zigzag to armchair free boundary is revealed. Aside from the topological wave mechanism, where edge transport occurs in the full gap for bulk wave and is protected by the bulk topology [45], the turning effect demonstrated originates from the coexistence of wave solutions on the zigzag and armchair edges over a certain frequency range.

The MGG is depicted in Fig. 1(a), where 820 stainless steel beads (diameter  $d = 7.95$  mm, Young’s modulus  $E = 190$  GPa and Poisson’s ratio  $\nu = 0.3$ ) are precisely placed in a honeycomb lattice, in contact with one another. This layout stems from a properly designed external magnetic field that is induced by permanent cylindrical NdFeB magnets (remanent magnetization  $B = 1.37$  T, diameter 6 mm, and length 13 mm) placed in a honeycomb configuration within the wood matrix, Fig. 1(b). The periodic external magnetic field magnetizes the elastic beads, resulting in equal pre-compression forces between them and a mechanically stable structure. Between the elastic beads and the substrate, a thin layer of rubber (thickness 2 mm) has been set to minimize the mechanical coupling of the granular graphene with the substrate, Fig. 1(b), and to damp the transmission of elastic waves into the wood matrix. The experimental set-up is shown in Fig. 1(c). In-plane motion is excited by the driver connected to a piezoelectric transducer (*Pana-*

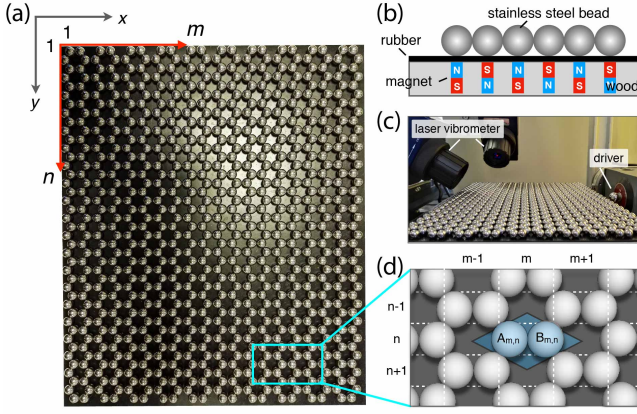


Figure 1. (a) Top view of the realistic MGG, composed of 820 beads. (b) Side view of the MGG. (c) Experimental setup for detecting wave propagation in the MGG. (d) Close-up of the MGG. The blue box highlights a unit cell at position  $(m,n)$  containing the two sublattice particles, labeled  $A$  and  $B$ .

metrics V3052). Each bead in the structure exhibits one out-of-plane rotation  $\varphi$  around the  $z$ -axis and two in-plane translations  $u$  and  $v$  along the  $x$ - and  $y$ -axes, respectively. The  $u$  and  $v$  components of each bead can be monitored separately by two laser vibrometers, which are sensitive to changes in the optical path length along the beam direction.

Between adjacent beads, we consider normal, shear and bending interactions, the rigidities of which can be obtained from Hertzian contact mechanics [46, 47], see supplemental materials (SM). As displayed in Fig. 1(d), the motion of particle  $A$  ( $B$ ) in normalized coordinates is labeled by  $U_{m,n} = [u_A; v_A; \Phi_A]_{m,n}$  ( $V_{m,n} = [u_B; v_B; \Phi_B]_{m,n}$ ), where  $\Phi = \varphi d/2$  and  $m, n$  are both integers representing the normalized center positions of beads in the  $x$ - and  $y$ -axes, respectively. On site  $(m, n)$ , the motion equations are expressed as:

$$\ddot{U}_{m,n} = S_0 U_{m,n} + S_1 V_{m,n} + S_2 V_{m-1,n+1} + S_3 V_{m-1,n-1}, \quad (1a)$$

$$\ddot{V}_{m,n} = D_0 V_{m,n} + D_1 U_{m,n} + D_2 U_{m+1,n+1} + D_3 U_{m+1,n-1}, \quad (1b)$$

where  $S_i$  and  $D_i$  ( $i = 0, 1, 2, 3$ ) are  $3 \times 3$  matrices (see SM). By applying the periodic boundary condition on Eqs. (1), the dispersion curves of an infinite MGG can be predicted, see Figs. 2(a) and (b). The MGG used in these experiments is of a size  $21 \times 41$  with free zigzag edges at positions  $(m, n) = (1, n)$ ,  $(m, n) = (21, n)$  and armchair edges at  $(m, n) = (m, 1)$ ,  $(m, n) = (m, 41)$ , which leads to the following boundary conditions:

$$M_0 V_{1,n} + D_1 U_{1,n} = 0, \quad (2a)$$

$$M_1 U_{21,n} + S_1 V_{21,n} = 0, \quad (2b)$$

for the zigzag edges, and,

$$M_2 U_{m,1} + S_3 V_{m-1,0} = 0, \quad (3a)$$

$$M_3 V_{m,1} + D_3 U_{m+1,0} = 0, \quad (3b)$$

$$M_4 U_{m,41} + S_2 V_{m-1,42} = 0, \quad (3c)$$

$$M_5 V_{m,41} + D_2 U_{m+1,40} = 0, \quad (3d)$$

for the armchair edges with  $M_j$  ( $j = 0, 1, 2, 3, 4, 5$ )  $3 \times 3$  matrices. To account for dissipation, a phenomenological on-site damping term has also been introduced into the right-hand side of the motion equations,  $-1/\tau \dot{U}_{m,n}$  ( $-1/\tau \dot{V}_{m,n}$ ) with  $\tau \sim 1$  ms in Eq. (1a) (Eq. (1b)). This coefficient has been chosen to fit the experimental results.

To measure the MGG dispersion, in-plane motion has been activated using a frequency sweep excitation from 500 Hz to 35 kHz by the bead-driver located at position  $(1, 22)$ . The  $u, v$  components of particle  $B$  in each unit cell are collected by the laser vibrometers. By scanning all particles  $B$ , the spatial frequency signals of translation can be obtained, which in turn yields the dispersion curves by applying a double Fourier transform. Figs. 2(a) and (b) present the dispersion curves of an infinite granular graphene without dissipation. The color scale level reflects the weights of  $u$  (red curves) and  $v$  (green curves) components in each mode. The corresponding numerical dispersion curves, mimicking the experimental process, are displayed in Figs. 2(c) and (d), while the experimental ones are shown in Figs. 2(e) and (f) for the  $u$  and  $v$  components respectively. Figs. 2(c)-(f) indicate that up to  $\sim 20$  kHz, the experimental dispersion curves are in good agreement with both the theoretical and numerical curves since the branches are translation-dominated. As expected, the branches with frequencies above  $\sim 20$  kHz are absent due to the fact that these modes are rotation-dominated and not easily detected by our laser vibrometers. Interestingly, Figs. 2(e) and (f) reveal the band crossing at the K point around frequency 10 kHz. The observation of this crossing provides evidence of the Dirac cone in MGG, originating from the honeycomb lattice symmetry (see SM for more details). Note that, another Dirac cone is also predicted around 24 kHz, Figs. 2(a) and (b). However, this Dirac point is not visible in experiments since the modes around 24 kHz are rotation-dominated.

Another interesting feature that appears in the dispersion of the finite-sized MGG is the existence of the branches in the MK directions around 20 kHz (green circles in Fig. 2(c)-(f)). These modes correspond to edge modes. By investigating the free boundaries in Eqs. (2) and (3), the edge wave dispersion for the zigzag and armchair edges are calculated, see Fig. 3(a) and (c), respectively. The gray regions correspond to bulk while

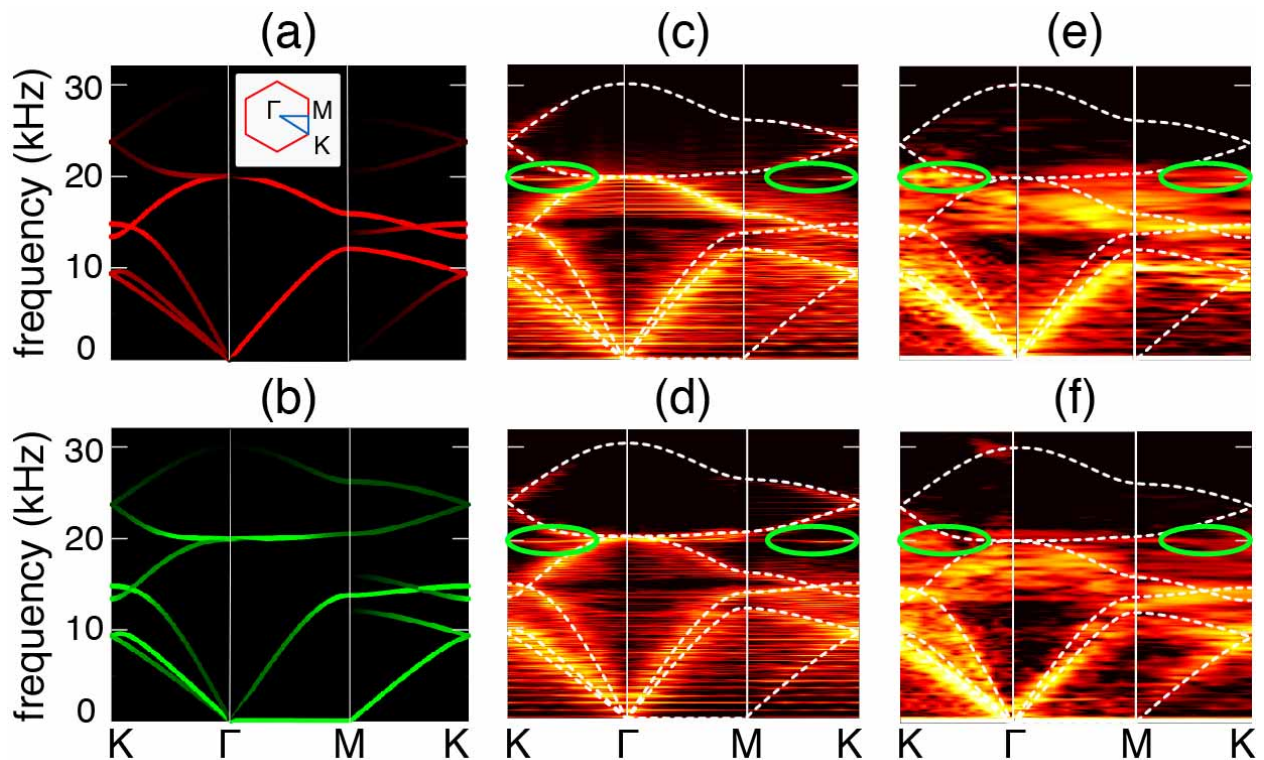


Figure 2. Dispersion relations of the MGG. (a), (b) Theoretical (infinite MGG), (c), (d) numerical (finite MGG), (e), (f) experimental dispersion relations. Panels (a), (c) and (e) show the dispersion curves of the  $u$  component, while the  $v$  component curves are presented in (b), (d) and (f).

the red (blue) curves to edge wave solutions. In all, 2 edge branches for the zigzag and 3 for the armchair are present. This increased number of edge states, and especially the existence of edge states at the armchair edge, is not encountered in the photonic analogues of graphene, thus enriching the edge physics of MGG. Fig. 3(b) and (d) present a close-up of the edge wave dispersion around 20 kHz for the zigzag and armchair cases, respectively. Note the overlapping region from  $\sim 19.84$  kHz to  $\sim 20.07$  kHz, where edge modes can be found on both the zigzag and armchair edges. To confirm this observation, the eigenmode of the finite-sized MGG at 19.889 kHz (green dots in Fig. 3(b) and (d)) is shown in Fig. 3(f). It is apparent that the motion is mainly confined on both zigzag and armchair edges. For comparison, another eigenmode at 19.621 kHz, which lies below the overlapping region (black dot in Fig. 3(b)), is shown in Fig. 3(g), indicating that this edge state is confined on the two zigzag edges. Finally, in Fig. 3(e), the eigenmode with frequency 24.820 kHz is presented. The color scales of the three components suggest that this mode is dominated by rotation.

The experimental set-up for edge wave measurement is the same as that shown in Fig. 1(c), while a harmonic signal of duration 10 ms with an initial linear ramping has been used as the source. All particles  $B$  are still scanned to record the  $u$ ,  $v$  components. Figure 4 displays the mea-

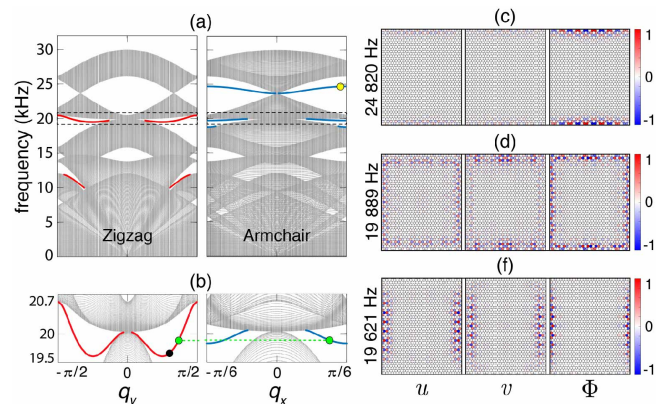


Figure 3. (a) Edge wave dispersion curves for the zigzag and armchair edges. (b) Zoom around 20 kHz. The gray regions represent the bulk modes, the red (blue) lines correspond to the edge wave branches. Amplitude distributions of the three components  $u$ ,  $v$  and  $\Phi$  of edge wave eigenmodes for three frequencies marked in the edge branches at: (c) 24.82 kHz by the yellow dot in (a), (d) 19.889 kHz by the green dots in (b), and (f) 19.621 kHz by the black dot in (b).

surements of total displacement amplitude ( $\sqrt{u^2 + v^2}$ ) for two separate times with the signal of 20 kHz. As shown in Fig. 4(a), when  $t = 1.7$  ms, the displacements

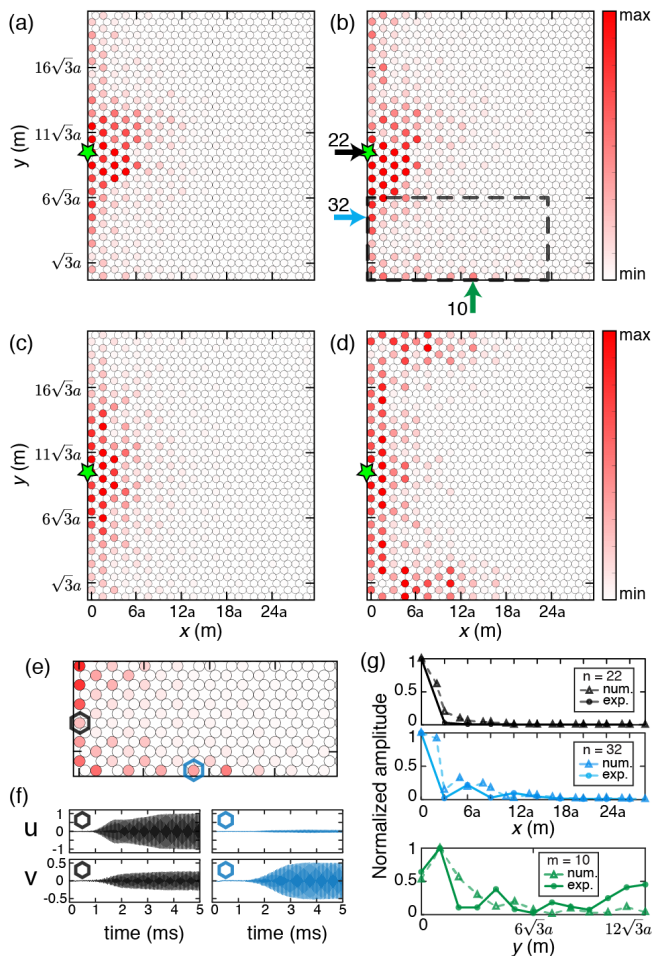


Figure 4. The spatiotemporal patterns of motion before the MGG reaches steady state are presented in (a) and (c), and after reaching steady state in (b) and (d). A harmonic wave at 20 kHz is excited from the source (green star). The experimental results are shown in (a), (b), while (c), (d) are the simulations. (e) Close-up of the corner marked by the dashed box in (b). (f) The temporal signals of the two particles highlighted by black and blue hexagons in (e). (g) Translation distributions of beads along row 22 (black), row 32 (blue) and column 10 (green), depicted by the arrows in (b)

are primarily localized on the zigzag edge while decaying into the bulk. Despite the excitation of bulk waves at this frequency, decay of the bulk wave is expected due to both dissipation and two-dimensional geometric spreading which provides a better observation of the elastic edge wave at 20 kHz. Numerically, the simulation of the experimental process is shown in Fig. 4(c), where the translational components of just the B particles is shown. A good agreement between experiment and simulation is achieved. The asymmetry of wave propagation in the upward and downward directions in the experiments is most likely due to uncertainties in the pre-compression forces and asymmetric excitation of motion due to small misalignment between the driving bead and the set-up.

Since edge modes are found in both zigzag and armchair edges at around 20 kHz, one expects that when the zigzag edge wave of 20 kHz reaches the corner, this wave can be mode-converted into an armchair edge wave. To observe this phenomenon, the spatial pattern at  $t = 3.7$  ms is depicted in Fig. 4(b) and (d). Indeed, wave motions are seen to be localized on both the zigzag and armchair edges. This can be further confirmed by the close-up of the experimental spatial pattern of motion at the lower MGG corner as presented in Fig. 4(e). To demonstrate this turning effect more clearly, we have chosen two particles marked by black and blue hexagons in Fig. 4(e) and studied their motion. In addition, Figure 4(g) provides greater detail for the spatial distribution of edge waves at a given point in time by focusing on rows  $n = 22$ ,  $n = 32$  and column  $m = 10$ , as labeled in Fig. 4(b) by arrows. As shown in Fig. 4(g), rows  $n = 22$  and  $n = 32$  produce similar results with the translational signals becoming very weak (the amplitude is normalized to the first bead on the left zigzag edge) after a distance of around  $x = 9a$ . For  $m = 10$ , i.e. bottom of Fig. 4(g), the translational signal also reveals a profile similar to those in rows  $n = 22$  and  $n = 32$ , thus confirming that bead movement in the armchair edge is due to the turning effect and not from the bulk modes (wave motions are basically localized near the armchair edge). Note that, as indicated in Figs. 4(b) and (d), due to dissipation and slow propagation velocity, the edge wave at 20 kHz on the armchair edge is damped before propagating a long distance, e.g.  $15a$ . Further investigation of zigzag and armchair edge wave dynamics both with and without losses can be found in the SM.

In conclusion, this work has studied the elastic wave properties in a finite-sized granular graphene. The dispersion curves and the Dirac cone signature have been measured. Moreover, a direct observation of edge wave propagation in MGG has been reported and a turning effect from zigzag to armchair edges have been revealed. The MGG proposed herein offers a perfect platform to explore nonlinear bulk and edge states. The study in this work also paves the way for future experiments in the field of topological elastic edge waves, while taking advantage of the special features of granular systems.

This work has been funded by RFI Le Mans Acoustique in the framework of the APAMAS and Sine City LMac projects and by the project CS.MICRO funded under the program Etoiles Montantes of the Region Pays de la Loire.

\* liyang.zheng.etu@univ-lemans.fr

† georgiostheocharis@gmail.com

- [1] A. H. C. Neto, F. Guinea, N. M. R. Peres, K. S. Novoselov, and A. K. Geim, *Rev. Mod. Phys.* **81**, 109 (2009).
- [2] S. D. Sarma, S. Adam, E. H. Hwang, and E. Rossi, *Rev. Mod. Phys.* **83**, 407 (2011).

- [3] A. K. Geim, and K. S. Novoselov, *Nature Mater.* **6**, 183191 (2007).
- [4] K. Wakabayashi, Ken-ichi Sasaki, T. Nakanishi and T. Enoki, *Sci. Technol. Adv. Mater.* **11** 054504 (2010).
- [5] Y. Kobayashi, K. Fukui, T. Enoki, K. Kusakabe, and Y. Kaburagi, *Phys. Rev. B* **71**, 193406 (2005).
- [6] A. V. Savin, and Y. S. Kivshar, *Phys. Rev. B* **81**, 165418 (2010).
- [7] M. Polini, F. Guinea, M. Lewenstein, H. C. Manoharan, and V. Pellegrini, *Nature Nanotechnology*, **8**, 625 (2013).
- [8] L. Tarruell, D. Greif, T. Uehlinger, G. Jotzu, and T. Esslinger, *Nature* **496**, 302 (2012).
- [9] M. C. Rechtsman, J. M. Zeuner, Y. Plotnik, Y. Lumer, D. Podolsky, F. Dreisow, S. Nolte, M. Segev, and A. Szameit, *Nature (London)* **496**, 196 (2013).
- [10] M. Dubois, C. Shi, X. Zhu, Y. Wang, and X. Zhang, *Nat. Commun.* **8**, 14871, (2017).
- [11] X. Zhang, and Z. Liu, *Phys. Rev. Lett.* **101**, 264303 (2008).
- [12] S.-Y. Yu, X.-C. Sun, X. Ni, Q. Wang, X.-J. Yan, C. He, X.-P. Liu, L. Feng, M.-H. Lu, and Y.-F. Chen, *Nature Mater.* **15**, 12431247 (2016).
- [13] M. J. Ablowitz, S. D. Nixon, and Y. Zhu, *Phys. Rev. A* **79**, 053830 (2009).
- [14] Si-Yuan Yu, Xiao-Chen Sun, Xu Ni, QingWang, Xue-Jun Yan, Cheng He, Xiao-Ping Liu, Liang Feng, Ming-Hui Lu, and Yan-Feng Chen, *Nature Mater.* ..., ... (2016).
- [15] D. Torrent, and J. Sanchez-Dehesa, *Phys. Rev. Lett.* **108**, 174301 (2012).
- [16] Y. Plotnik, M.C. Rechtsman, D. Song, M. Heinrich, J.M. Zeuner, S. Nolte, Y. Lumer, N. Malkova, J. Xu, A. Szameit, Z. Chen, and M. Segev, *Nature Mater.* **13**, 5762 (2014).
- [17] M. Bellec, U. Kuhl, G. Montambaux, and F. Mortessagne, *New J. Phys.* **16**, 113023 (2014).
- [18] J.-W. Dong, X.-D. Chen, H. Zhu, Y. Wang, and X. Zhang, *Nat. Mater.* **10**, 3945 (2014).
- [19] R. Fleury, A. B. Khanikaev, and A. Alu, *Nat. Commun.* **7**, 11744 (2016).
- [20] H. Abbaszadeh, A. Souslov, J. Paulose, H. Schomerus, and V. Vitelli, *Phys. Rev. Lett.* **119**, 195502 (2017).
- [21] Y. Liu, C.-S. Lian, Y. Li, Y. Xu, and W. Duan, *Phys. Rev. Lett.* **119**, 255901 (2017).
- [22] C. Brendel, V. Peano, O. J. Painter, and F. Marquardt, *Proc. Natl. Acad. Sci.*, **114** (17) E3390-E3395 (2017).
- [23] M. Milicevic, T. Ozawa, G. Montambaux, I. Carusotto, E. Galopin, A. Lematre, L. Le Gratiet, I. Sagnes, J. Bloch, and A. Amo, *Phys. Rev. Lett.* **118**, 107403 (2017).
- [24] T. Kariyado and Y. Hatzugai, *Sci. Reports* **5**, 18107 (2015).
- [25] V. Tournat, I. Pèrez-Arjona, A. Merkel, V Sanchez-Morcillo, and V. Gusev, *New J. Phys.* **13**, 073042 (2011).
- [26] L.-Y. Zheng, H. Pichard, V. Tournat, G. Theocharis, and V. Gusev, *Ultrasonics* **69**, 201214 (2016).
- [27] L.-Y. Zheng, G. Theocharis, V. Tournat, and V. Gusev, *Phys. Rev. B* **97**, 060101(R) (2018).
- [28] A. Merkel, V. Tournat, V. Gusev, *Phys. Rev. Lett.* **107**, 225502 (2011).
- [29] M. Hiraiwa, M. Abi Ghanem, S. P. Wallen, A. Khanolkar, A. A. Maznev, and N. Boechler, *Phys. Rev. Lett.* **116**, 198001 (2016).
- [30] H. Pichard, A. Duclos, J.-P. Groby, and V. Tournat, *Phys. Rev. B* **86**, 134307 (2012).
- [31] F. Allein, V. Tournat, V. E. Gusev, and G. Theocharis, *Appl. Phys. Lett.* **108**, 161903 (2016).
- [32] C. Chong, M. A. Porter, P. G. Kevrekidis, and C. Daraio, *J. Phys. Condens. Matter* **29**, 413002 (2017).
- [33] V.F. Nesterenko, *Dynamics of Heterogeneous Materials*, Springer-Verlag, New York, 2001.
- [34] C. Coste, E. Falcon, and S. Fauve, *Phys. Rev. E* **56**, 6104-6117 (1997).
- [35] S. Job, F. Melo, A. Sokolow, and S. Sen, *Phys. Rev. Lett.* **94**, 178002 (2005).
- [36] A. Leonard, and C. Daraio, *Phys. Rev. Lett.* **108**, 214301 (2012).
- [37] A. Leonard, F. Fraternali, and C. Daraio, *Exp. Mech.* **53**, 327337 (2013).
- [38] J. Cabaret, P. Béquin, G. Theocharis, V. Andreev, V. E. Gusev, and V. Tournat, *Phys. Rev. Lett.* **115**, 054301 (2015).
- [39] N. Boechler, G. Theocharis, S. Job, P. G. Kevrekidis, Mason A. Porter, and C. Daraio, *Phys. Rev. Lett.* **104**, 244302 (2010).
- [40] G. Theocharis, M. Kavousanakis, P. G. Kevrekidis, C. Daraio, M. A. Porter, and I. G. Kevrekidis, *Phys. Rev. E* **80**, 066601 (2009).
- [41] L.-Y. Zheng, V. Tournat, and V. Gusev, *Extreme Mechanics Letters* **12**, 5564 (2017).
- [42] B. Gilles, and C. Coste, *Phys. Rev. Lett.* **90**, 174302 (2003).
- [43] C. Coste, and B. Gilles, *Phys. Rev. E* **77**, 021302 (2008).
- [44] A. Leonard, C. Daraio, *Phys. Rev. Lett.* **108**, 214301, 2012
- [45] H. Zhu, T.-W. Liu, and F. Semperlotti, *Phys. Rev. B* **97**, 174301 (2018).
- [46] K. L. Johnson, *Contact Mechanics*, Cambridge Univ. Press, 1985.
- [47] R. D. Mindlin, *Trans. ASME J. Appl. Mech.* **16**, 259 (1949).